

X marks the spot: accurate energies from intersecting extrapolations of continuum quantum Monte Carlo data

Seyed Mohammadreza Hosseini,¹ Ali Alavi,^{1,2} and Pablo López Ríos^{1, a)}

¹⁾Max-Planck Institute for Solid State Research, Heisenbergstr. 1, 70569 Stuttgart, Germany

²⁾Yusuf Hamied Department of Chemistry, University of Cambridge, Lensfield Road, Cambridge CB2 1EW, UK

We explore the application of an extrapolative method that yields very accurate total and relative energies from variational and diffusion quantum Monte Carlo (VMC and DMC) results. For a trial wave function consisting of a small configuration interaction (CI) wave function obtained from full CI quantum Monte Carlo and reoptimized in the presence of a Jastrow factor and an optional backflow transformation, we find that the VMC and DMC energies are smooth functions of the sum of the squared coefficients of the initial CI wave function, and that quadratic extrapolations of the non-backflow VMC and backflow DMC energies intersect within uncertainty of the exact total energy. With adequate statistical treatment of quasi-random fluctuations, the *extrapolate and intersect with polynomials of order two* (XSPOT) method is shown to yield results in agreement with benchmark-quality total and relative energies for the C₂, N₂, CO₂, and H₂O molecules, as well as for the C₂ molecule in its first electronic singlet excited state, using only small CI expansion sizes.

I. INTRODUCTION

Quantum Monte Carlo (QMC) methods are a broad family of stochastic wave-function-based techniques that accurately approximate the solution of the Schrödinger equation of an electronic system. The variational quantum Monte Carlo (VMC) method^{1,2} obtains expectation values corresponding to an analytic trial wave function $\Psi_T(\mathbf{R})$ in real space and provides a framework for optimizing wave function parameters,^{3,4} such as those in the multideterminant-Jastrow-backflow form,

$$\Psi_T(\mathbf{R}) = e^{J(\mathbf{R})} \sum_I^M c_I D_I[\mathbf{X}(\mathbf{R})], \quad (1)$$

where $\{D_I\}$ are M Slater determinants, $e^{J(\mathbf{R})}$ is a Jastrow correlation factor,^{5,6} and $\mathbf{X}(\mathbf{R})$ are backflow-transformed electronic coordinates.⁷ Diffusion quantum Monte Carlo (DMC)^{2,8} is a real-space projection method which recovers the lowest-energy solution $\Phi(\mathbf{R})$ of the Schrödinger equation compatible with the fixed-node condition that $\Phi(\mathbf{R})\Psi_T(\mathbf{R})$ be nonnegative everywhere. We refer to the VMC and DMC methods collectively as continuum QMC (cQMC) methods.

In the configuration interaction (CI) ansatz the solution of the Schrödinger equation is expressed as

$$|\Psi\rangle = \sum_I c_I |D_I\rangle, \quad (2)$$

where $\{|D_I\rangle\}$ are all possible Slater determinants that can be constructed in a given orbital basis. Equation 2 is exact in the limit of an infinite expansion using a complete basis set, but in practical methods finite expansions and bases are used. Full CI quantum Monte Carlo (FCIQMC)^{9,10} is a second-quantized projection technique in which random walkers sample the discrete Hilbert space defined by $\{|D_I\rangle\}$ in order to determine approximate values of the CI coefficients $\{c_I\}$.

The nominal computational cost of cQMC calculations scales polynomially with system size N , typically as N^2-N^4 , and the quality of the resulting energies depends on the accuracy of the trial wave function for VMC, and on the accurate location of its nodes for DMC. The cQMC methods excel at describing explicit dynamic and long-ranged correlations, but the error incurred by the fixed-node approximation is often significant. By contrast, FCIQMC is formally an exponentially-scaling method which trivially captures static correlations, but requires a very large number of walkers to provide a good description of dynamic correlations. The complementary nature of the strengths of cQMC and FCIQMC makes combining these methods highly desirable. Several ways of combining cQMC and FCIQMC have been presented in the literature, such as using DMC to assist in the extrapolation to the thermodynamic limit of FCIQMC energies of the electron gas,¹¹ or using VMC-optimized Jastrow factors in FCIQMC with the transcorrelated method.^{12,13} Here we shall focus on the use of selected CI wave functions generated with FCIQMC to construct multideterminantal trial wave functions for cQMC calculations.

Multideterminant expansions have been used for decades in cQMC calculations of atomic and molecular systems, including ground-state energy calculations,¹⁴⁻¹⁹ excitation energies,²⁰⁻²³ and geometry optimizations.^{22,24} The use of truncated CI expansions in cQMC presents the problem that no reliable criteria exist to truncate wave functions for different systems in a consistent manner, resulting in energy differences of questionable accuracy. One possible approach is to use extremely large multideterminantal wave functions,¹⁹⁻²⁷ under the expectation that the fixed-node error in the total energies will become smaller than the target error. While algorithmic developments have vastly reduced the computational cost associated with the use of multideterminantal wave functions in cQMC,^{25,28-31} this remains an expensive choice. Using trial wave functions without a Jastrow factor reduces the nominal computational burden^{20,21,27} at the cost of losing the accurate, compact description of dynamic correlation afforded by fully-optimized trial wave functions. By including explicit

^{a)}Electronic mail: p.lopez.rios@fkf.mpg.de

correlations, in the present paper we are able to explore the use of relatively small multideterminantal wave functions to perform an extrapolation of the cQMC total energy to the full-CI, complete orbital-basis limit. We test our method on a variety of molecular systems, obtaining total and relative energies within uncertainty of benchmark-quality results from the literature.

The rest of this paper is structured as follows. In Section II we present the methodological details of our extrapolation method, which we illustrate with calculations of the carbon dimer and the water molecule. We then apply our method to several atomic and molecular systems, and we report the results in Section III. Our conclusions and outlook are presented in Section IV. Hartree atomic units ($\hbar = |e| = m_e = 4\pi\epsilon_0 = 1$) are used throughout; the uncertainties and error bars we report refer to standard 68.3% (one-sigma) confidence intervals except when explicitly noted otherwise.

II. METHODOLOGY

Let M_{gen} be the number of determinants occupied at a given point in an equilibrated FCIQMC calculation, representing the CI wave function

$$|\Psi_{M_{\text{gen}}}\rangle = \sum_{I=1}^{M_{\text{gen}}} c_I |D_I\rangle, \quad (3)$$

where c_I is obtained as the sum of the signed weights of the walkers occupying the I th determinant. The values of the first few coefficients $\{c_I\}_{I \ll M_{\text{gen}}}$ converge relatively quickly in FCIQMC calculations and can be expected to be reasonably close to their full CI (FCI) values. This makes FCIQMC an ideal method for quickly generating good-quality selected CI wave functions of moderate sizes – studying the suitability of other CI solvers for this purpose is beyond the scope of this paper.

Let us consider the wave function obtained by truncating Eq. 3 to size $M \ll M_{\text{gen}}$. The sum of the squares of the coefficients of the resulting wave function relative to that at size M_{gen} is

$$w^2 = \frac{\sum_{I=1}^M c_I^2}{\sum_{I=1}^{M_{\text{gen}}} c_I^2}, \quad (4)$$

which goes to 1 as $M \rightarrow M_{\text{gen}}$. This CI wave function of size M can be combined with a Jastrow factor, and optionally with a backflow transformation, to produce a multideterminant-Jastrow(-backflow) trial wave function for cQMC, as given in Eq. 1. The wave function parameters can be (re-)optimized in the context of VMC, producing a trial wave function with which to compute VMC and DMC energies. Repeating this procedure by truncating the original CI wave function to different sizes yields a set of VMC and DMC energies that can be plotted as a function of w .

Plots of this kind, albeit using other CI solvers, can be found in the literature; see Fig. 3 of Ref. 4 or Fig. 4 of Ref. 29, for

example. The present work is in fact inspired by the observation that the VMC and DMC curves in these plots appear to be smooth and would seem to be about to intersect just off the right-hand side of the graph. In Fig. 1 we plot the VMC and DMC energies we obtain for the ground state of the all-electron C_2 molecule, see Table I, using Hartree-Fock orbitals expanded in the cc-pCVTZ basis set,^{32,33} along with quadratic fits to the data of the form

$$E(w) = a + bw + cw^2, \quad (5)$$

where a , b , and c are fit parameters. In this simple example,

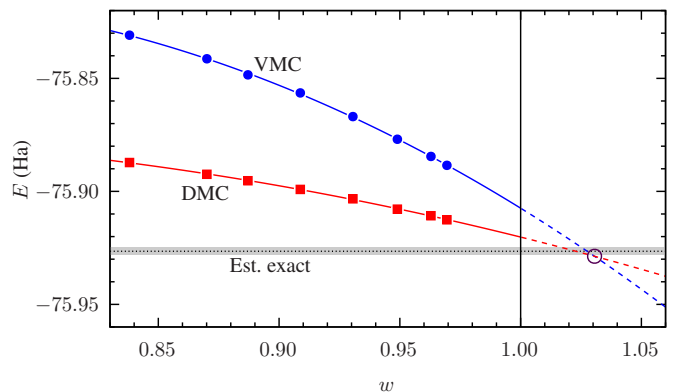


FIG. 1. VMC and DMC total ground-state energy of the carbon dimer using multideterminant-Jastrow trial wave functions as a function of w , using Hartree-Fock orbitals expanded in the cc-pCVTZ basis set. Quadratic fits to the data are extended beyond $w = 1$ to show their intersection, which is in good agreement with the estimated exact nonrelativistic total energy of the system.³⁴

the fits to the VMC and DMC data intersect at $w = 1.031$, corresponding to a total energy of -75.9287 Ha, not far off the exact nonrelativistic total energy estimate of -75.9265 Ha given in Ref. 34. We refer to this way of estimating the total energy of a system as the *extrapolate and intersect with polynomials of order two* (XSPOT) method.

In what follows we develop the methodology to enable the application of the XSPOT method in practice using as test systems the C, N, and O atoms, the ground-state C_2 , N_2 , H_2O , and CO_2 molecules, and the C_2 molecule in its lowest-lying singlet electronic excited state, which we refer to simply as C_2^* . These atoms and molecules are simulated as all-electron, both in the sense that no effective-core potentials are used and that excitations from “core” orbitals are allowed in the CI wave function. In Table I we give the states and geometries we have used for these systems.

A. Theoretical justification

The extrapolation shown in Fig. 1 might seem simplistic from a quantum chemical perspective, given that all calculations involved have been performed with the same, finite-orbital basis, so one would expect an orbital-basis dependent result which should itself be extrapolated to the complete-basis

System	Geometry ^{34,35}	State
C		3P
N		4S
O		3P
C ₂	$r_{CC} = 1.2425 \text{ \AA}$	$^1\Sigma_g^+$
C ₂ *	$r_{CC} = 1.2425 \text{ \AA}$	$B^1\Delta_g$
H ₂ O	$r_{OH} = 0.9572 \text{ \AA}$ $\angle_{HOH} = 104.5^\circ$	1A_1
N ₂	$r_{NN} = 1.0977 \text{ \AA}$	$^1\Sigma_g^+$
CO ₂	$r_{CO} = 1.1600 \text{ \AA}$ $\angle_{OCO} = 180^\circ$	$^1\Sigma_g^+$

TABLE I. Atoms and molecules considered in this work, along with their electronic states and geometries.

limit. For instance, the FCIQMC energy tends to a basis-set dependent FCI limit as the number of walkers tends to infinity, and this must in turn be extrapolated to the basis-set limit in order to obtain the exact energy of the system.

In what follows we will conceptually combine the choice of molecular orbitals (e.g., Hartree-Fock, natural orbitals, ...) with the choice of basis set (e.g., cc-pCVDZ, cc-aug-pVTZ, ...), so we shall discuss the completeness of the (molecular) orbital basis instead of that of the basis set alone to emphasize this point.

The XSPOT extrapolation procedure can be easily justified in the hypothetical case of using an infinite, “complete” orbital basis. The FCIQMC energy with this “complete” orbital basis would tend to the exact total energy of the system E_0 in the infinite walker-number limit, and the sum of the squared CI coefficients would also tend to that of the exact wave function, w_0 . The exact wave function has no dynamic correlation left to recover, so the Jastrow factor and backflow displacement in the cQMC trial wave function would optimize to zero, and the VMC and DMC energies would both coincide with E_0 . At finite expansion sizes, $w < w_0$, the VMC and DMC methods yield variational energies satisfying $E_{VMC} \geq E_{DMC} \geq E_0$, which, assuming these to be smooth functions of w , validates the XSPOT method with the “complete” orbital basis.

We note that in a truncated CI wave function, the infinite, “complete” orbital basis is effectively finite, since a finite number of determinants can only contain a finite number of distinct orbitals. Conversely, a sufficiently small selected CI wave function with a finite orbital basis is indistinguishable from a CI wave function of the same size with the “complete” orbital basis – assuming the finite basis contains the first few orbitals in the “complete” orbital basis.

As the orbitals in a finite basis get used up, the cQMC energies can be expected to plateau as a function of w as they tend to their orbital-basis dependent limit. We refer to this phenomenon as “orbital-basis exhaustion”, and to the onset of this plateau as the exhaustion limit $w_{\text{exh.}}$. Note that orbital bases such as natural orbitals can be constructed so as to compactly describe the system with fewer orbitals, which has the side effect of reducing the value of $w_{\text{exh.}}$. We discuss this aspect further in Section II C.

As a proxy for the degree of orbital-basis exhaustion, in Table II we show the fraction of orbitals used in CI wave functions of the same size for Hartree-Fock orbitals expanded in four different basis sets in the cc-pV x Z and cc-pCV x Z families^{32,33} for the all-electron carbon dimer. Based on these

Basis set	Orbitals used
cc-pVDZ	28/28 = 100%
cc-pCVDZ	32/36 = 89%
cc-pVTZ	38/60 = 82%
cc-pCVTZ	40/86 = 47%

TABLE II. Fraction of spatial orbitals in the Hartree-Fock orbital basis expanded in each of four basis sets that appear in the first 300 configuration state functions of the full CI wave function for the ground state of the carbon dimer.

numbers, we use the cc-pCVTZ basis throughout this paper to ensure we have enough leeway to increase the multideterminant wave function size before hitting the exhaustion limit. We provide an *a posteriori* assessment of this choice in Section III.

Finite-orbital-basis FCIQMC and cQMC calculations performed at $w < w_{\text{exh.}}$ behave as if one were using the “complete” orbital basis. Therefore it is legitimate to expect that the extrapolation of quadratic fits to these VMC and DMC data intersect at $w = w_0$ and $E = E_0$, provided that the VMC and DMC energies are smooth functions of w representable by a second-order polynomial for $w_{\text{h.o.}} < w < w_{\text{exh.}}$, where $w_{\text{h.o.}}$ is a threshold below which higher-order polynomials would be needed.

Note that the initial FCIQMC wave function with M_{gen} determinants is not required to be below the exhaustion limit since it simply serves to construct selected CI wave functions of size $M \ll M_{\text{gen}}$, which are required to be below the exhaustion limit, and to define the arbitrary point at which $w = 1$ in the plots; $w = 1$ has no special significance in this method.

In our calculations we choose CI wave function sizes so that the points are more or less evenly spaced in the w axis, and we make sure that different points correspond to wave functions containing a different number of distinct spatial orbitals so as to capture the effect of simultaneously growing the CI expansion and the orbital basis.

B. Obtaining statistically meaningful results

In reality cQMC energies do not exactly follow smooth curves, but it is reasonable to assume that a smooth underlying trend $E(w)$ exists, and that the cQMC energy E_i deviates from it by a quasi-random amount q_i . Considering also the statistical uncertainty ΔE_i , the i th point in a set of cQMC energies can then be modelled as

$$E_i = E(w_i) + q_i + \zeta_i \Delta E_i, \quad (6)$$

where ζ_i is a random number drawn from the standard normal distribution. In order to make this generic model for the quasi-

random fluctuations useful in practice, we make the approximation that $q_i = \xi_i \alpha$, where ξ_i is a random number drawn from the standard normal distribution and α is a constant amplitude independent of w . In Fig. 2 we illustrate our model of cQMC energy data as a function of w .

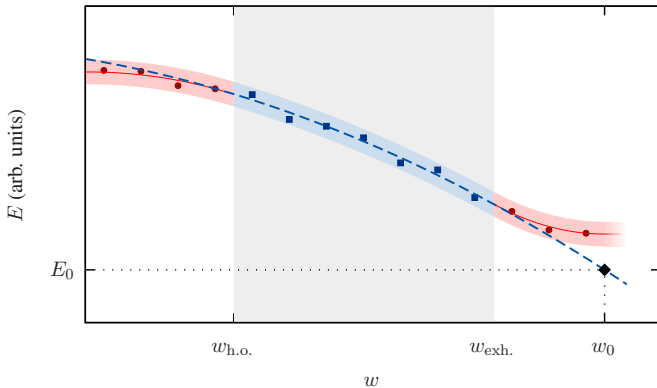


FIG. 2. Illustration of the expected behavior of cQMC energies as a function of w . The cQMC energies (circles and squares) deviate from the underlying smooth trend (lines) by a quasirandom amount (of amplitude represented by the width of the shaded area around the lines). The smooth trend can be represented by a quadratic function, $E(w)$ (dashed line), for $w_{h.o.} < w < w_{exh.}$ (shaded middle region), while for $w < w_{h.o.}$ higher-order contributions become important, and for $w > w_{exh.}$ orbital-basis exhaustion sets in. At the value of w corresponding to the exact wave function the quadratic function gives the exact energy, $E_0 = E(w_0)$.

We estimate the value of α by performing a preliminary least-squares fit to the bare data, $\tilde{E}(w)$, and evaluating

$$\alpha^2 = \max\left(0, \left\langle \left[E_i - \tilde{E}(w_i) \right]^2 \right\rangle - \left\langle (\Delta E_i)^2 \right\rangle \right), \quad (7)$$

i.e., we obtain α as the root-mean-square deviation of the data from the fit value *not accounted for by statistical uncertainty alone*. For this procedure to produce a meaningful result, the number of data points in each curve must be significantly greater than the number of parameters in the quadratic fit function; we use at least 7 data points for all fits reported in this paper.

In order to account for the statistical uncertainty and quasirandom fluctuations in the XSPOT method, we use a Monte Carlo resampling technique in which we generate 100 000 instances of each VMC and DMC dataset in which a random amount proportional to $\sqrt{\alpha^2 + \Delta E_i^2}$ is added to the original energy values. We then perform fits to these shifted data and find the intersection point for each such instance, and obtain the final result by averaging over instances; see Fig. 3 for an illustration of this process. This procedure provides meaningful uncertainties on the intersection energies which account for both the cQMC statistical uncertainty and quasi-random deviations from the smooth trend.

We demonstrate the full statistical procedure of the XSPOT method on multideterminant-Jastrow data for the carbon dimer in Fig. 4. Notice that the distribution of intersection

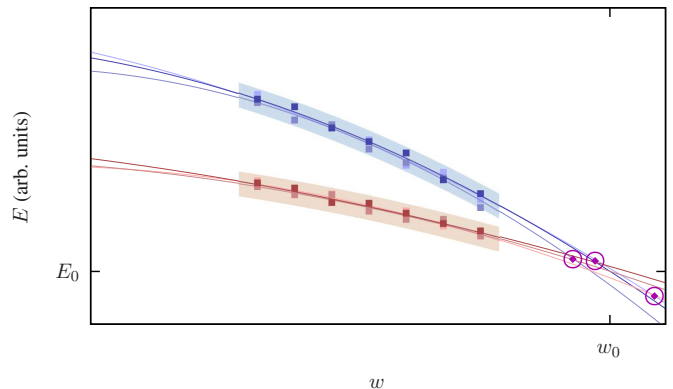


FIG. 3. Illustration of the Monte Carlo resampling scheme used to compute statistics on the intersection between two curves. For each curve, having obtained an estimate of α (width of the shaded region) from the original energy data (not shown), we create a synthetic instance of the dataset by shifting the original points by a random amount proportional to $\sqrt{\alpha^2 + \Delta E_i^2}$ (squares of same color saturation), perform a quadratic fit (line), and find the intersection between both fits (circled diamond). This process is repeated over the random instances (three shown in the illustration), from which statistics on the intersection are obtained.

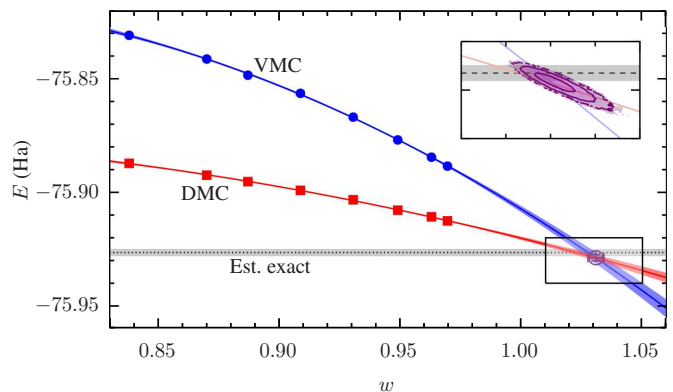


FIG. 4. VMC and DMC energies of the ground-state C_2 molecule as a function of w , as shown in Fig. 1, using the full statistical treatment of the XSPOT method. Mean values of the fits to the data are shown as lines, and the translucent areas around them represent 95.5% (two-sigma) confidence intervals. Also shown is the estimated exact nonrelativistic energy³⁴ as a dotted line with a shaded area of ± 1 kcal/mol around it, and the intersection point between the curves. The inset shows the statistical distribution of intersection points as a color map with overlaid contour curves.

points shown in the inset of Fig. 4 has a tail extending towards low E and large w . These tails become more problematic the more parallel the two intersecting curves are, eventually preventing the evaluation of an intersection point at all. It is therefore important to try to apply the XSPOT method to curves which are as close to perpendicular as possible.

In Fig. 5 we include additional VMC and DMC data using an inhomogeneous backflow transformation (“bVMC” and “bDMC”) for the carbon dimer. We list the intersections between pairs of curves in Table III, all of which are within un-

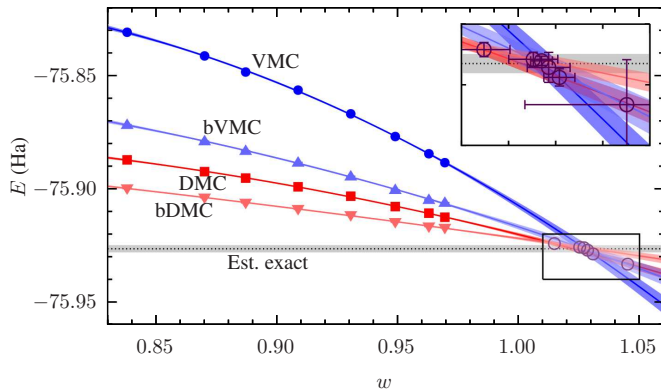


FIG. 5. VMC, DMC, bVMC, and bDMC energies of the ground-state C_2 molecule as a function of w . Mean values of the fits to the data are shown as lines, and the translucent areas around them represent 95.5% (two-sigma) confidence intervals. Also shown is the estimated exact nonrelativistic energy³⁴ as a dotted line with a shaded area of ± 1 kcal/mol around it, and the intersection points between each of the six possible pairs of curves; error bars on these are only shown in the inset for clarity.

certainty of each other. The VMC and bDMC curves provide

Curves	w_0	E_0 (a.u.)	Miss (%)
VMC-DMC	1.031(3)	-75.9288 ± 0.0014	0.00
VMC-bVMC	1.028(5)	-75.9271 ± 0.0025	0.00
VMC-bDMC	1.027(2)	-75.9260 ± 0.0008	0.00
DMC-bVMC	1.05(2)	-75.9333 ± 0.0074	2.75
DMC-bDMC	1.015(6)	-75.9242 ± 0.0012	0.00
bVMC-bDMC	1.025(5)	-75.9258 ± 0.0012	0.00

TABLE III. Location of all six pairwise intersections of the VMC, DMC, bVMC, and bDMC curves shown in Fig. 5 for the C_2 molecule. “Missed intersections” refer to random instances of the curves that do not intersect at $w > 1$ in the Monte Carlo resampling procedure.

the best-resolved results, which is to be expected since these curves intersect at the widest angle among all pairs of curves, as can be seen in Fig. 5. By contrast, the DMC and bVMC curves intersect at a narrow angle and incur a small but non-zero fraction of “missed” intersections, i.e., random instances of the data whose fits fail to intersect at $w > 1$, which signals the presence of heavy tails in the intersection distribution, resulting in a large uncertainty on the intersection energy.

For the four curves in Fig. 5, the estimated amplitude of the quasi-random fluctuations ranges from $\alpha = 0.17$ to 0.41 mHa. Throughout this paper we converge the cQMC calculations so that the uncertainties satisfy $\langle (\Delta E_i)^2 \rangle < \alpha^2$, i.e., so that quasirandom fluctuations represent the main contribution to the uncertainty on the fits and intersections; see the supplementary material for the list of values of α obtained. The statistical uncertainties on the cQMC energies can thus be neglected for all practical purposes.

C. Choice of orbital basis

As alluded to in Section II A, the choice of molecular orbitals plays a crucial role in the behavior of the cQMC energies as a function of w , modifying the point $w_{\text{exh.}}$ at which the effects of exhaustion start to become noticeable. In Fig. 6 we demonstrate this for the H_2O molecule by comparing the cQMC energies obtained using Hartree-Fock orbitals expanded in the cc-pCVTZ basis set and natural orbitals expanded in the same basis set constructed so as to diagonalize the one-body density matrix in coupled cluster singles and doubles (CCSD). While CCSD natural orbitals produce lower cQMC energies and correspond to larger values of w at fixed expansion sizes, the cQMC energies we obtain using Hartree-Fock orbitals follow the quadratic trend throughout the whole w range considered, while those obtained with natural orbitals plateau very early on, preventing their meaningful extrapolation.

III. RESULTS AND DISCUSSION

A. Calculation details

In our calculations we use Hartree-Fock orbitals expanded in the cc-pCVTZ Gaussian basis set^{32,33} obtained using MOLPRO.³⁶ We perform a small-scale FCIQMC calculation using the NECI package³⁷ with configuration state functions (CSFs) instead of determinants as walker sites,³⁸ which reduces the number of FCIQMC walkers required to accurately represent the wave function; note that the use of CSFs is not a requirement of the XSPOT method. The FCIQMC population is grown to 10^6 walkers and equilibrated, and the coefficients of the $M_{\text{gen}} = 10\,000$ most-occupied CSFs are recorded from a population snapshot. From this information we build CI expansions with the M CSFs with largest absolute coefficients, where $M \leq 1500 \ll M_{\text{gen}}$. In our cQMC calculations the orbitals are corrected to obey the electron-nucleus cusp condition.³⁹

The CSF coefficients are reoptimized in the presence of a Jastrow factor of the Drummond-Towler-Needs form,^{5,6} and of an optional inhomogeneous backflow transformation including electron-electron, electron-nucleus, and electron-electron-nucleus terms.⁷ We do not optimize any of the parameters in the molecular orbitals, which provide degrees of freedom that overlap significantly with those in the backflow transformation. Note that even though CSFs are used, the presence of the Jastrow factor and of the backflow transformation prevents the cQMC trial wave function from formally being an exact spin state.⁴⁰ We optimize our wave function parameters using linear least-squares energy minimization^{3,4} with 10^6 statistically independent VMC-generated electronic configurations, a number large enough that the optimized cQMC energy can be assumed to lie reasonably close to its variational minimum; note that any remaining optimization error can be considered to be absorbed into the quasirandom error.

The resulting trial wave function is then used to run two

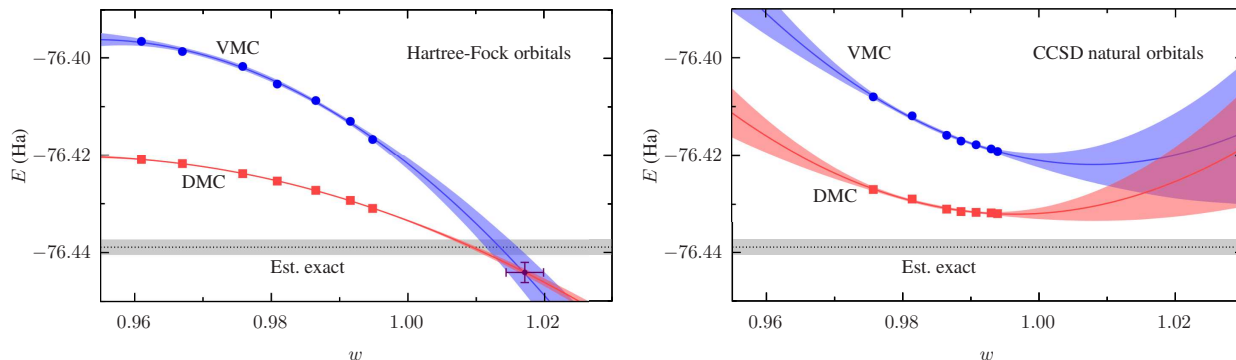


FIG. 6. VMC and DMC energies of the H_2O molecule as a function of w , both using Hartree-Fock orbitals (left) and CCSD natural orbitals (right) expanded in the cc-pCVTZ basis set. In both cases the same numbers of CSFs are used. Mean values of the fits to the data are shown as lines, and the translucent areas around them represent 95.5% (two-sigma) confidence intervals. Also shown is the estimated exact nonrelativistic energy³⁵ as a dotted line with a shaded area of ± 1 kcal/mol around it, and the intersection point between the VMC and DMC curves in the left panel. The cQMC energies obtained with natural orbitals plateau with w , preventing the quadratic extrapolations from reaching the exact energy.

DMC calculations with time steps 0.001 and 0.004 a.u. and target populations of 2048 and 512 configurations, respectively, except for bDMC runs on CO_2 at 500 and 1000 CSFs for which we use 65536 and 16384 configurations. These energies are then linearly extrapolated to the zero time-step, infinite-population limit.^{2,41}

We use the CASINO package² to run the cQMC calculations, and use multi-determinant compression³⁰ to reduce the computational expense of evaluating the trial wave function. We perform the fits to the data and find their intersections using our custom POLYFIT tool.⁴² The cQMC energies obtained for all systems can be found in the supplementary material.

B. Results

In this section we test the XSPOT method on all eight systems under consideration to assess the different aspects discussed in Section II and to determine the broader applicability of the method. The VMC and bDMC energies and fits we obtain for the eight systems are shown in Fig. 7; additional plots containing the bVMC and DMC energies can be found in the supplementary material.

All the curves in Fig. 7 are relatively smooth and provide a well-defined intersection. The apparent non-monotonicity of the bDMC curve for the carbon atom is an artifact of the use of a fit function which formally allows non-monotonic behavior, and should be interpreted accordingly: $E(w)$ can be regarded to approach the intersection with negligible slope, and the region $w > w_0$ should be ignored since $E(w)$ does not have a physical meaning there. All of the other fits appear to be monotonic in the range shown.

The fraction of orbitals used, a proxy for the degree of orbital-basis exhaustion, is plotted for each of the systems in Fig. 8. We do not use up all of the orbitals in the basis in any of our calculations, and the curves in Fig. 7 do not seem to exhibit symptoms of orbital-basis exhaustion. The bVMC energies do seem to plateau somewhat, which we discuss briefly

in the supplementary material; note that we do not use the bVMC data to obtain our final results.

In Table IV we compare the total energies obtained from applying the XSPOT method to VMC and bDMC energy data with benchmark-quality estimates of the exact nonrelativistic energies of the systems from the literature, along with our best bDMC result and prior cQMC results for reference. The atomization energies of the ground-state molecules are shown in Table V. For excited-state C_2^* we compare the vertical excitation energy with that calculated with internally-contracted multi-reference coupled cluster theory (ic-MRCC);⁴⁴⁻⁴⁶ we have computed the total energy of C_2^* shown in Table IV by adding the ic-MRCC excitation energy to the estimated ground-state energy of C_2 from Ref. 34.

All of the total energies reported in Table IV are within statistical uncertainty of their corresponding benchmark values. An important observation is that our individual cQMC energies are not lower than those from prior cQMC calculations, implying that we incur a lower computational cost, but our XSPOT results are in general closer to the benchmarks than cQMC results from prior studies. Our XSPOT energies are on average 1.1 standard errors above the benchmark, with a root-mean-square deviation of 1.9 standard errors. These results are compatible with the XSPOT method being exact when the method's assumptions are satisfied. The relative energies are likewise in agreement with the benchmark values.

We find that the magnitude α of the quasi-random fluctuations of the cQMC energies is of up to 0.7 mHa. These fluctuations are particularly visible in the VMC data for N, O, and H_2O in Fig. 7, for example; in the supplementary material we give the values of α we have obtained for each of the curves. The magnitude of the quasirandom fluctuations does not seem to increase too rapidly with system size, but their effect on the extrapolated energy becomes more pronounced the further the cQMC data are from the intersection in the plots. This increasing uncertainty on the XSPOT total energies, reaching 4 mHa for the CO_2 molecule, hints at a limitation of the methodology: the cQMC energies and values of w ob-

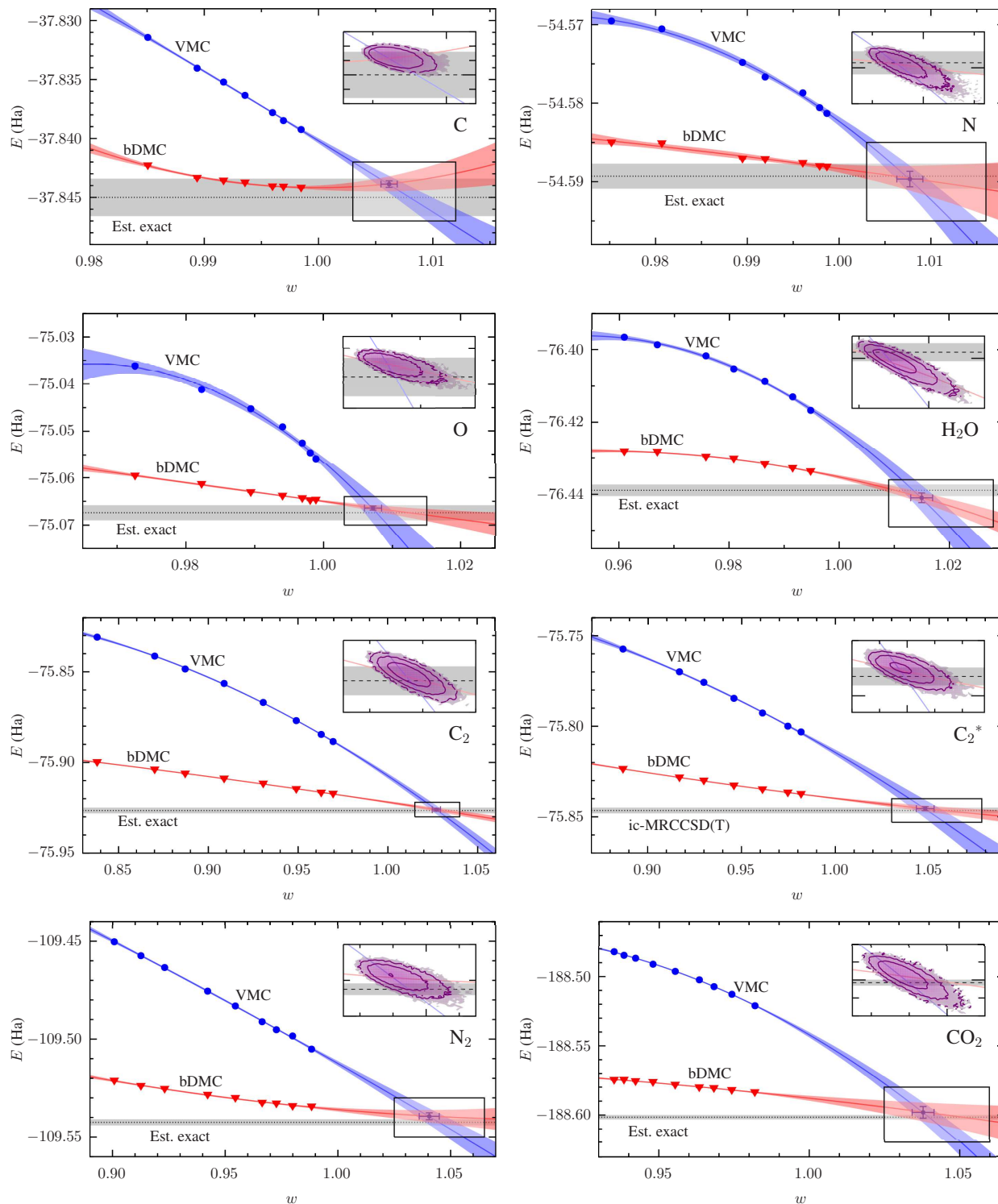


FIG. 7. VMC and bDMC energies of the atoms and molecules considered in this work as a function of w . Mean values of the fits to the data are shown as lines, and the translucent areas around them represent 95.5% (two-sigma) confidence intervals. Also shown in each plot is the relevant benchmark energy (see details in text and Table IV) as a dotted line with a shaded area of ± 1 kcal/mol around it, and the intersection point between the VMC and bDMC curves. The insets show the statistical distributions of intersection points as color maps with overlaid contour curves.

tained using modest-sized multideterminant expansions with a fixed basis set move away from the intersection point with

increasing system size, which in turn exacerbates the effects of quasirandom noise on the uncertainty of the XSPOT energy;

System	Prior cQMC	Our best bDMC	XSPOT	Benchmark
C	-37.84438(5) ^a	-37.8442(0)	-37.8439 ± 0.0003	-37.8450 ^b
N	-54.58829(7) ^a	-54.5881(0)	-54.5897 ± 0.0014	-54.5893 ^b
O	-75.06591(8) ^a	-75.0647(1)	-75.0664 ± 0.0004	-75.0674 ^b
H ₂ O	-76.4389(1) ^d	-76.4336(1)	-76.4410 ± 0.0013	-76.4389 ^c
C ₂	-75.9229(6) ^a	-75.9172(1)	-75.9260 ± 0.0008	-75.9265 ^b
C ₂ *		-75.8374(1)	-75.8455 ± 0.0011	-75.8465 ^{e,b}
N ₂	-109.5372(3) ^a	-109.5344(1)	-109.5394 ± 0.0018	-109.5425 ^c
CO ₂		-188.5837(2)	-188.5981 ± 0.0042	-188.6015 ^c

^aRef. 18; ^bRef. 34; ^cRef. 35; ^dRef. 43; ^eRefs. 44–46.

TABLE IV. Total energies in Ha obtained with the XSPOT method using the VMC and bDMC data for the various atoms and molecules considered in this work, along with results from prior multi-determinant cQMC studies, our best individual bDMC energy for each system, and benchmark-quality nonrelativistic total energies from the literature.

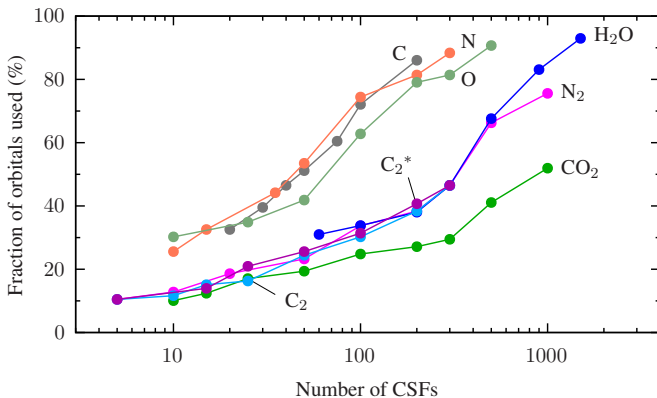


FIG. 8. Number of distinct spatial orbitals in the FCIQMC trial wave functions relative to that in the orbital basis as a function of the number of CSFs, for the various systems considered in this work.

	XSPOT	Benchmark
H ₂ O → 2H + O	374.6 ± 1.4	371.4 ^b
C ₂ → 2C	238.3 ± 0.9	236.5 ^a
C ₂ → C ₂ *	80.6 ± 1.3	80.0 ^c
N ₂ → 2N	360.1 ± 2.3	363.9 ^b
CO ₂ → C + 2O	621.4 ± 4.3	621.7 ^b

^aRef. 34; ^bRef. 35; ^cRefs. 44–46.

TABLE V. Atomization and excitation energies in mHa of the various molecules considered in this work corresponding to the total energies in Table IV obtained from the XSPOT method, along with benchmark-quality nonrelativistic relative energies from the literature.

one would have to use bigger basis sets and larger multiterminantal expansions to get data closer to the intersection in order to reduce this uncertainty, increasing the computational cost of the approach.

IV. CONCLUSIONS

We have presented an empirical extrapolation strategy for cQMC energies as a function of the sum of the squared multiterminantal coefficients in the initial selected CI wave function from which the trial wave function is constructed. This approach is made possible by the smoothness of the energies as a function of the CI expansion size, and we have presented a simple statistical procedure to handle the quasi-random non-smoothness in the data, which we show to work very well in practice. We find that Hartree-Fock orbitals expanded in standard basis sets provide the type of gradual convergence required for the XSPOT method to work well. The results from the tests we have conducted are compatible with the XSPOT method being capable of obtaining exact total energies, with the caveat that trial wave function complexity must increase with system size in order to control the uncertainty on the results.

SUPPLEMENTARY MATERIAL

See the supplementary material for the cQMC data used in this paper, a table of the magnitude of the quasirandom fluctuations encountered, and discussion of connected extrapolation approaches. The supplementary material additionally cites Refs. 1–5.

ACKNOWLEDGMENTS

P.L.R. and A.A. acknowledge support from the European Centre of Excellence in Exascale Computing TREX, funded by the Horizon 2020 program of the European Union under grant no. 952165. Views and opinions expressed are those of the authors only and do not necessarily reflect those of the European Union or the European Research Executive Agency. Neither the European Union nor the granting authority can be held responsible for them.

¹W. L. McMillan, *Ground State of Liquid He⁴*, *Phys. Rev.* **138**, A442 (1965).

- ²R. J. Needs, M. D. Towler, N. D. Drummond, P. López Ríos, and J. R. Trail, *Variational and diffusion quantum Monte Carlo calculations with the CASINO code*, *J. Chem. Phys.* **152**, 154106 (2020).
- ³J. Toulouse and C. J. Umrigar, *Optimization of quantum Monte Carlo wave functions by energy minimization*, *J. Chem. Phys.* **126**, 084102 (2007).
- ⁴C. J. Umrigar, J. Toulouse, C. Filippi, S. Sorella, and R. G. Hennig, *Alleviation of the fermion-sign problem by optimization of many-body wave functions*, *Phys. Rev. Lett.* **98**, 110201 (2007).
- ⁵N. D. Drummond, M. D. Towler, and R. J. Needs, *Jastrow correlation factor for atoms, molecules, and solids*, *Phys. Rev. B* **70**, 235119 (2004).
- ⁶P. López Ríos, P. Seth, N. D. Drummond, and R. J. Needs, *Framework for constructing generic Jastrow correlation factors*, *Phys. Rev. E* **86**, 036703 (2012).
- ⁷P. López Ríos, A. Ma, N. D. Drummond, M. D. Towler, and R. J. Needs, *Inhomogeneous backflow transformations in quantum Monte Carlo calculations*, *Phys. Rev. E* **74**, 066701 (2006).
- ⁸D. M. Ceperley and B. J. Alder, *Ground State of the Electron Gas by a Stochastic Method*, *Phys. Rev. Lett.* **45**, 566 (1980).
- ⁹G. H. Booth, A. J. W. Thom, and A. Alavi, *Fermion Monte Carlo without fixed nodes: A game of life, death, and annihilation in Slater determinant space*, *J. Chem. Phys.* **131**, 054106 (2009).
- ¹⁰D. Cleland, G. H. Booth, and A. Alavi, *Survival of the fittest: accelerating convergence in full configuration interaction quantum Monte Carlo*, *J. Chem. Phys.* **132**, 041103 (2010).
- ¹¹M. Ruggeri, P. López Ríos, and A. Alavi, *Correlation energies of the high-density spin-polarized electron gas to meV accuracy*, *Phys. Rev. B* **98**, 161105(R) (2018).
- ¹²A. J. Cohen, H. Luo, K. Guthrie, W. Dobrutz, D. P. Tew, and Ali Alavi, *Similarity transformation of the electronic Schrödinger equation via Jastrow factorization*, *J. Chem. Phys.* **151**, 061101 (2019).
- ¹³J. P. Haupt, S. M. Hosseini, P. López Ríos, W. Dobrutz, A. Cohen, and A. Alavi, *Optimizing Jastrow factors for the transcorrelated method*, *J. Chem. Phys.* **158**, 224105 (2023).
- ¹⁴C. Filippi and C. J. Umrigar, *Multiconfiguration wave functions for quantum Monte Carlo calculations of first-row diatomic molecules*, *J. Chem. Phys.* **105**, 213 (1996).
- ¹⁵M. D. Brown, J. R. Trail, P. López Ríos, and R. J. Needs, *Energies of the first row atoms from quantum Monte Carlo*, *J. Chem. Phys.* **126**, 224110 (2007).
- ¹⁶P. Seth, P. López Ríos, and R. J. Needs, *Quantum Monte Carlo study of the first-row atoms and ions*, *J. Chem. Phys.* **134**, 084105 (2011).
- ¹⁷F. R. Petruzielo, Julien Toulouse, and C. J. Umrigar, *Approaching chemical accuracy with quantum Monte Carlo*, *J. Chem. Phys.* **136**, 124116 (2012).
- ¹⁸M. A. Morales, J. McMinis, B. K. Clark, J. Kim, G. E. Scuseria, *Multideterminant wave functions in quantum Monte Carlo*, *J. Chem. Theory Comput.* **8**, 2181 (2012).
- ¹⁹E. Giner, R. Assaraf, and J. Toulouse, *Quantum Monte Carlo with re-optimised perturbatively selected configuration-interaction wave functions*, *Mol. Phys.* **114**, 910 (2016).
- ²⁰A. Scemama, A. Benali, D. Jacquemin, M. Caffarel, and P.-F. Loos, *Excitation energies from diffusion Monte Carlo using selected configuration interaction nodes*, *J. Chem. Phys.* **149**, 034108 (2018).
- ²¹A. Scemama, M. Caffarel, A. Benali, D. Jacquemin, and P.-F. Loos, *Influence of pseudopotentials on excitation energies from selected configuration interaction and diffusion Monte Carlo*, *Res. Chem.* **1**, 100002 (2019).
- ²²M. Dash, J. Feldt, S. Moroni, A. Scemama, and C. Filippi, *Excited states with selected configuration interaction-quantum Monte Carlo: chemically accurate excitation energies and geometries*, *J. Chem. Theory Comput.* **15**, 4896 (2019).
- ²³M. Dash, S. Moroni, C. Filippi, and A. Scemama, *Tailoring CIPSI expansions for QMC calculations of electronic excitations: the case study of thiophene*, *J. Chem. Theory Comput.* **17**, 3426 (2021).
- ²⁴M. Dash, S. Moroni, A. Scemama, and C. Filippi, *Perturbatively selected configuration-interaction wave functions for efficient geometry optimization in quantum Monte Carlo*, *J. Chem. Theory Comput.* **14**, 4176 (2018).
- ²⁵A. Scemama, T. Applencourt, E. Giner, M. Caffarel, *Quantum Monte Carlo with very large multideterminant wavefunctions*, *J. Comput. Chem.* **37**, 1866 (2016).
- ²⁶M. C. Per, and D. M. Cleland, *Energy-based truncation of multi-determinant wavefunctions in quantum Monte Carlo*, *J. Chem. Phys.* **146**, 164101 (2017).
- ²⁷A. Scemama, Y. Garniron, M. Caffarel, and P.-F. Loos, *Deterministic construction of nodal surfaces within quantum Monte Carlo: the case of FeS*, *J. Chem. Theory Comput.* **14**, 1395 (2018).
- ²⁸P. K. V. V. Nukala and P. R. C. Kent, *A fast and efficient algorithm for Slater determinant updates in quantum Monte Carlo simulations*, *J. Chem. Phys.* **130**, 204105 (2009).
- ²⁹B. K. Clark, M. A. Morales, J. McMinis, J. Kim, and G. E. Scuseria, *Computing the energy of a water molecule using multideterminants: a simple, efficient algorithm*, *J. Chem. Phys.* **135**, 244105 (2011).
- ³⁰G. L. Weerasinghe, P. López Ríos, and R. J. Needs, *Compression algorithm for multi-determinant wave functions*, *Phys. Rev. E* **89**, 023304 (2014).
- ³¹C. Filippi, R. Assaraf, and S. Moroni, *Simple formalism for efficient derivatives and multi-determinant expansions in quantum Monte Carlo*, *J. Chem. Phys.* **144**, 194105 (2016).
- ³²T. H. Dunning Jr., *Gaussian basis sets for use in correlated molecular calculations. I. The atoms boron through neon and hydrogen*, *J. Chem. Phys.* **90**, 1007 (1989).
- ³³D. E. Woon and T. H. Dunning Jr., *Gaussian basis sets for use in correlated molecular calculations. V. Core-valence basis sets for boron through neon*, *J. Chem. Phys.* **103**, 4572 (1995).
- ³⁴L. Bytautas and K. Ruedenberg, *Correlation energy extrapolation by intrinsic scaling. IV. Accurate binding energies of the homonuclear diatomic molecules carbon nitrogen, oxygen, and fluorine*, *J. Chem. Phys.* **122**, 154110 (2005).
- ³⁵D. Feller, K. A. Peterson, and D. A. Dixon, *A survey of factors contributing to accurate theoretical predictions of atomization energies and molecular structures*, *J. Chem. Phys.* **129**, 204105 (2008).
- ³⁶H.-J. Werner, P. J. Knowles, F. R. Manby, J. A. Black, K. Doll, A. Heßelmann, D. Kats, A. Köhn, T. Korona, D. A. Kreplin, Q. Ma, T. F. Miller III, A. Mitrushchenkov, K. A. Peterson, I. Polyak, G. Rauhut, and M. Sibae, *The Molpro quantum chemistry package*, *J. Chem. Phys.* **152**, 144107 (2020).
- ³⁷K. Guthrie, R. J. Anderson, N. S. Blunt, N. A. Bogdanov, D. Cleland, N. Dattani, W. Dobrutz, K. Ghanem, P. Jeszenszki, N. Liebermann, G. Li Manni, A. Y. Lozovoi, H. Luo, D. Ma, F. Merz, C. Overy, M. Rampp, P. K. Samanta, L. R. Schwarz, J. J. Shepherd, S. D. Smart, E. Vitale, O. Weser, G. H. Booth, and A. Alavi, *NECI: N-electron configuration interaction with an emphasis on state-of-the-art stochastic methods*, *J. Chem. Phys.* **153**, 034107 (2020).
- ³⁸W. Dobrutz, S. D. Smart, and A. Alavi, *Efficient formulation of full configuration interaction quantum Monte Carlo in a spin eigenbasis via the graphical unitary group approach*, *J. Chem. Phys.* **151**, 094104 (2019).
- ³⁹A. Ma, M. D. Towler, N. D. Drummond, and R. J. Needs, *Scheme for adding electron-nucleus cusps to Gaussian orbitals*, *J. Chem. Phys.* **122**, 224322 (2005).
- ⁴⁰C.-J. Huang, C. Filippi, and C. J. Umrigar, *Spin contamination in quantum Monte Carlo wave functions*, *J. Chem. Phys.* **108**, 8838 (1998).
- ⁴¹R. M. Lee, G. J. Conduit, N. Nemeč, P. López Ríos, and N. D. Drummond, *Strategies for improving the efficiency of quantum Monte Carlo calculations*, *Phys. Rev. E* **83**, 066706 (2011).
- ⁴²Our custom regression tool can be found online at <https://github.com/plopezrios/polyfit>.
- ⁴³M. Caffarel, T. Applencourt, E. Giner, A. Scemama, *Communication: Toward an improved control of the fixed-node error in quantum Monte Carlo: The case of the water molecule*, *J. Chem. Phys.* **144**, 151103 (2016).
- ⁴⁴P. K. Samanta, private communication.
- ⁴⁵P. K. Samanta, D. Mukherjee, M. Hanauer, and A. Köhn, *Excited states with internally contracted multireference coupled-cluster linear response theory*, *J. Chem. Phys.* **140**, 134108 (2014).
- ⁴⁶M. Hanauer and A. Köhn, *Pilot applications of internally contracted multireference coupled cluster theory, and how to choose the cluster operator properly*, *J. Chem. Phys.* **134**, 204111 (2011).
- ⁴⁷A. A. Holmes, C. J. Umrigar, S. Sharma, *Excited states using semistochastic heat-bath configuration interaction*, *J. Chem. Phys.* **147**, 164111 (2017).
- ⁴⁸H. G. A. Burton, P.-F. Loos, *Rationale for the extrapolation procedure in selected configuration interaction*, *J. Chem. Phys.* **160**, 104102 (2024).
- ⁴⁹D. M. Ceperley, *The statistical error of Green's function Monte Carlo*, *J. Stat. Phys.* **43**, 815 (1986).
- ⁵⁰M. Taddei, M. Ruggeri, S. Moroni, and M. Holzmann, *Iterative backflow renormalization procedure for many-body ground-state wave functions of strongly interacting normal Fermi liquids*, *Phys. Rev. B* **91**, 115106 (2015).

⁵¹W. Fu, W. Ren, and J. Chen, *Variance extrapolation method for neural-network variational Monte Carlo*,

[Mach. Learn.: Sci. Technol. 5, 015016 \(2024\)](#).

Supplemental information for “X marks the spot: accurate energies from intersecting extrapolations of continuum quantum Monte Carlo data”

S1. VMC AND DMC DATA

Tables S1–S8 contain the cQMC energies we have obtained for our manuscript. These energies are plotted in Fig. S1, as Fig. 4 of the manuscript with added backflow VMC and non-backflow DMC curves.

The bVMC energy curves in Fig. S1 would appear to plateau somewhat at large w , a potential symptom of orbital-basis exhaustion. We hypothesize that the backflow transformation makes some of the information contained in the orbitals redundant, which effectively reduces the value of w_{exh} . with respect to the non-backflow data. Judging by the quality of the intersections, this issue affects bVMC more than it does bDMC, which would imply that this redundancy does not involve the location of the nodes of the trial wave function to the same degree as its values away from the nodes. This is in any case a tentative explanation; we do not use the bVMC data to obtain our final results.

n_{CSF}	n_{det}	n_{orb}	w	VMC	DMC	bVMC	bDMC
20	45	14	0.9851	-37.83143(2)	-37.83996(6)	-37.83884(2)	-37.84228(3)
30	68	17	0.9894	-37.83404(2)	-37.84157(6)	-37.84039(2)	-37.84335(3)
40	87	20	0.9917	-37.83522(2)	-37.84197(5)	-37.84068(2)	-37.84358(3)
50	109	22	0.9936	-37.83635(2)	-37.84250(5)	-37.84106(2)	-37.84374(3)
75	155	26	0.9960	-37.83781(2)	-37.84316(4)	-37.84146(2)	-37.84407(3)
100	222	31	0.9969	-37.83849(2)	-37.84342(4)	-37.84167(2)	-37.84409(3)
200	476	37	0.9985	-37.83924(2)	-37.84375(4)	-37.84219(2)	-37.84418(3)
Benchmark					-37.8450		

TABLE S1. VMC, DMC, bVMC, and bDMC energies for the C atom obtained for our manuscript, in Hartree atomic units. n_{CSF} is the number of CSFs in the wave function, n_{det} is the number of (not necessarily unique) determinants, and n_{orb} is the number of orbitals from the 43-orbital basis used in the wave function.

n_{CSF}	n_{det}	n_{orb}	w	VMC	DMC	bVMC	bDMC
10	19	11	0.9752	-54.56953(7)	-54.58134(7)	-54.58010(6)	-54.58501(4)
15	29	14	0.9807	-54.57054(7)	-54.58192(7)	-54.58067(6)	-54.58512(4)
35	77	19	0.9895	-54.57482(7)	-54.58464(6)	-54.58314(6)	-54.58708(6)
50	96	23	0.9919	-54.57667(6)	-54.58557(6)	-54.58363(6)	-54.58713(5)
100	189	32	0.9960	-54.57869(6)	-54.58632(6)	-54.58414(6)	-54.58762(4)
200	479	35	0.9979	-54.58057(6)	-54.58702(5)	-54.58477(6)	-54.58802(4)
300	761	38	0.9987	-54.58131(7)	-54.58729(5)	-54.58503(6)	-54.58808(4)
Benchmark					-54.5893		

TABLE S2. VMC, DMC, bVMC, and bDMC energies for the N atom obtained for our manuscript, in Hartree atomic units. n_{CSF} is the number of CSFs in the wave function, n_{det} is the number of (not necessarily unique) determinants, and n_{orb} is the number of orbitals from the 43-orbital basis used in the wave function.

n_{CSF}	n_{det}	n_{orb}	w	VMC	DMC	bVMC	bDMC
10	20	13	0.9726	-75.0362(1)	-75.0536(1)	-75.05225(9)	-75.05959(5)
25	61	15	0.9823	-75.0412(1)	-75.0571(1)	-75.05488(9)	-75.06135(4)
50	121	18	0.9894	-75.0452(1)	-75.0594(1)	-75.05701(9)	-75.06307(5)
100	244	27	0.9940	-75.0491(1)	-75.0611(1)	-75.05851(9)	-75.06384(5)
200	538	34	0.9969	-75.0525(1)	-75.0626(1)	-75.05928(9)	-75.06434(5)
300	856	35	0.9981	-75.0546(1)	-75.0634(1)	-75.06013(9)	-75.06476(5)
500	1598	39	0.9989	-75.0558(1)	-75.0639(1)	-75.06029(9)	-75.06467(5)
Benchmark					-75.0674		

TABLE S3. VMC, DMC, bVMC, and bDMC energies for the O atom obtained for our manuscript, in Hartree atomic units. n_{CSF} is the number of CSFs in the wave function, n_{det} is the number of (not necessarily unique) determinants, and n_{orb} is the number of orbitals from the 43-orbital basis used in the wave function.

n_{CSF}	n_{det}	n_{orb}	w	VMC	DMC	bVMC	bDMC
60	190	22	0.9610	-76.39663(3)	-76.4209(8)	-76.4159(1)	-76.42825(7)
100	338	24	0.9670	-76.3987(1)	-76.4218(8)	-76.4162(1)	-76.42836(7)
200	702	27	0.9758	-76.4018(1)	-76.4239(8)	-76.4190(1)	-76.42968(7)
300	1079	33	0.9809	-76.4054(1)	-76.4254(7)	-76.4198(1)	-76.43022(8)
500	1798	48	0.9865	-76.4088(1)	-76.4273(7)	-76.4218(1)	-76.43167(7)
900	3298	59	0.9916	-76.4130(1)	-76.4293(6)	-76.4241(1)	-76.43272(8)
1500	5698	66	0.9948	-76.4167(1)	-76.4310(6)	-76.4255(1)	-76.43362(8)
Benchmark					-76.4389		

TABLE S4. VMC, DMC, bVMC, and bDMC energies for the H₂O molecule obtained for our manuscript, in Hartree atomic units. n_{CSF} is the number of CSFs in the wave function, n_{det} is the number of (not necessarily unique) determinants, and n_{orb} is the number of orbitals from the 71-orbital basis used in the wave function.

n_{CSF}	n_{det}	n_{orb}	w	VMC	DMC	bVMC	bDMC
5	16	9	0.8381	-75.83089(7)	-75.8872(1)	-75.8718(2)	-75.8998(1)
10	28	10	0.8701	-75.84133(7)	-75.8924(1)	-75.87903(8)	-75.90389(9)
15	44	13	0.8871	-75.84845(7)	-75.8953(1)	-75.88329(7)	-75.90615(9)
25	68	14	0.9088	-75.85644(6)	-75.8991(1)	-75.8885(1)	-75.90891(9)
50	162	21	0.9306	-75.86691(6)	-75.9033(1)	-75.8946(1)	-75.91166(8)
100	350	26	0.9490	-75.87693(6)	-75.9079(1)	-75.9005(1)	-75.91468(7)
200	730	33	0.9629	-75.88454(6)	-75.9108(1)	-75.9049(1)	-75.91665(7)
300	1160	40	0.9695	-75.88847(6)	-75.9126(1)	-75.9062(1)	-75.91724(7)
Benchmark					-75.9265		

TABLE S5. VMC, DMC, bVMC, and bDMC energies for the ground-state C₂ molecule obtained for our manuscript, in Hartree atomic units. n_{CSF} is the number of CSFs in the wave function, n_{det} is the number of (not necessarily unique) determinants, and n_{orb} is the number of orbitals from the 86-orbital basis used in the wave function.

n_{CSF}	n_{det}	n_{orb}	w	VMC	DMC	bVMC	bDMC
5	7	9	0.8869	-75.75737(8)	-75.8116(1)	-75.7904(1)	-75.82356(8)
15	37	12	0.9170	-75.76993(8)	-75.8179(1)	-75.8016(1)	-75.82828(9)
25	75	18	0.9299	-75.77575(8)	-75.8203(1)	-75.80570(9)	-75.83000(8)
50	167	22	0.9460	-75.78458(8)	-75.8243(1)	-75.81104(9)	-75.83274(8)
100	348	27	0.9612	-75.79267(8)	-75.82662(9)	-75.81616(9)	-75.8348(1)
200	690	35	0.9747	-75.79994(8)	-75.83013(8)	-75.82048(8)	-75.83661(9)
300	1080	40	0.9817	-75.80313(7)	-75.83142(8)	-75.82172(8)	-75.8374(1)
Benchmark				-75.8465			

TABLE S6. VMC, DMC, bVMC, and bDMC energies for the excited-state C_2^* molecule obtained for our manuscript, in Hartree atomic units. n_{CSF} is the number of CSFs in the wave function, n_{det} is the number of (not necessarily unique) determinants, and n_{orb} is the number of orbitals from the 86-orbital basis used in the wave function.

n_{CSF}	n_{det}	n_{orb}	w	VMC	DMC	bVMC	bDMC
5	13	9	0.9008	-109.4503(1)	-109.5073(2)	-109.4957(1)	-109.52120(9)
10	23	11	0.9126	-109.4574(1)	-109.5111(1)	-109.5000(1)	-109.5239(1)
20	71	16	0.9231	-109.4634(1)	-109.5137(2)	-109.5029(1)	-109.5254(1)
50	177	20	0.9422	-109.4755(1)	-109.5180(1)	-109.5090(1)	-109.5284(1)
100	355	29	0.9545	-109.4831(1)	-109.5208(1)	-109.5126(1)	-109.5300(1)
200	748	33	0.9664	-109.4911(1)	-109.5243(1)	-109.5167(1)	-109.5325(1)
300	1145	40	0.9727	-109.4952(1)	-109.5259(2)	-109.5179(1)	-109.5329(1)
500	1199	57	0.9799	-109.4984(1)	-109.5270(2)	-109.5203(1)	-109.5342(1)
1000	4148	65	0.9883	-109.5051(1)	-109.5299(2)	-109.5216(1)	-109.5344(1)
Benchmark				-109.5425			

TABLE S7. VMC, DMC, bVMC, and bDMC energies for the N_2 molecule obtained for our manuscript, in Hartree atomic units. n_{CSF} is the number of CSFs in the wave function, n_{det} is the number of (not necessarily unique) determinants, and n_{orb} is the number of orbitals from the 86-orbital basis used in the wave function.

n_{CSF}	n_{det}	n_{orb}	w	VMC	DMC	bVMC	bDMC
10	23	13	0.9352	-188.48208(8)	-188.5546(2)	-188.54035(8)	-188.5748(1)
15	43	16	0.9384	-188.48468(8)	-188.5556(2)	-188.54091(8)	-188.5748(1)
25	85	22	0.9423	-188.48678(8)	-188.5567(2)	-188.54247(8)	-188.5758(1)
50	191	25	0.9481	-188.49112(8)	-188.5582(2)	-188.54495(8)	-188.5764(1)
100	390	32	0.9555	-188.49628(8)	-188.5600(2)	-188.54827(8)	-188.5784(1)
200	820	35	0.9635	-188.50237(8)	-188.5623(2)	-188.55245(9)	-188.5802(2)
300	1205	38	0.9684	-188.50730(8)	-188.5641(2)	-188.55395(9)	-188.5807(2)
500	2016	53	0.9743	-188.51281(8)	-188.5667(2)	-188.5567(1)	-188.5821(2)
1000	4177	67	0.9820	-188.52106(9)	-188.5709(1)	-188.5591(1)	-188.5837(2)
Benchmark				-188.6015			

TABLE S8. VMC, DMC, bVMC, and bDMC energies for the CO_2 molecule obtained for our manuscript, in Hartree atomic units. n_{CSF} is the number of CSFs in the wave function, n_{det} is the number of (not necessarily unique) determinants, and n_{orb} is the number of orbitals from the 129-orbital basis used in the wave function.

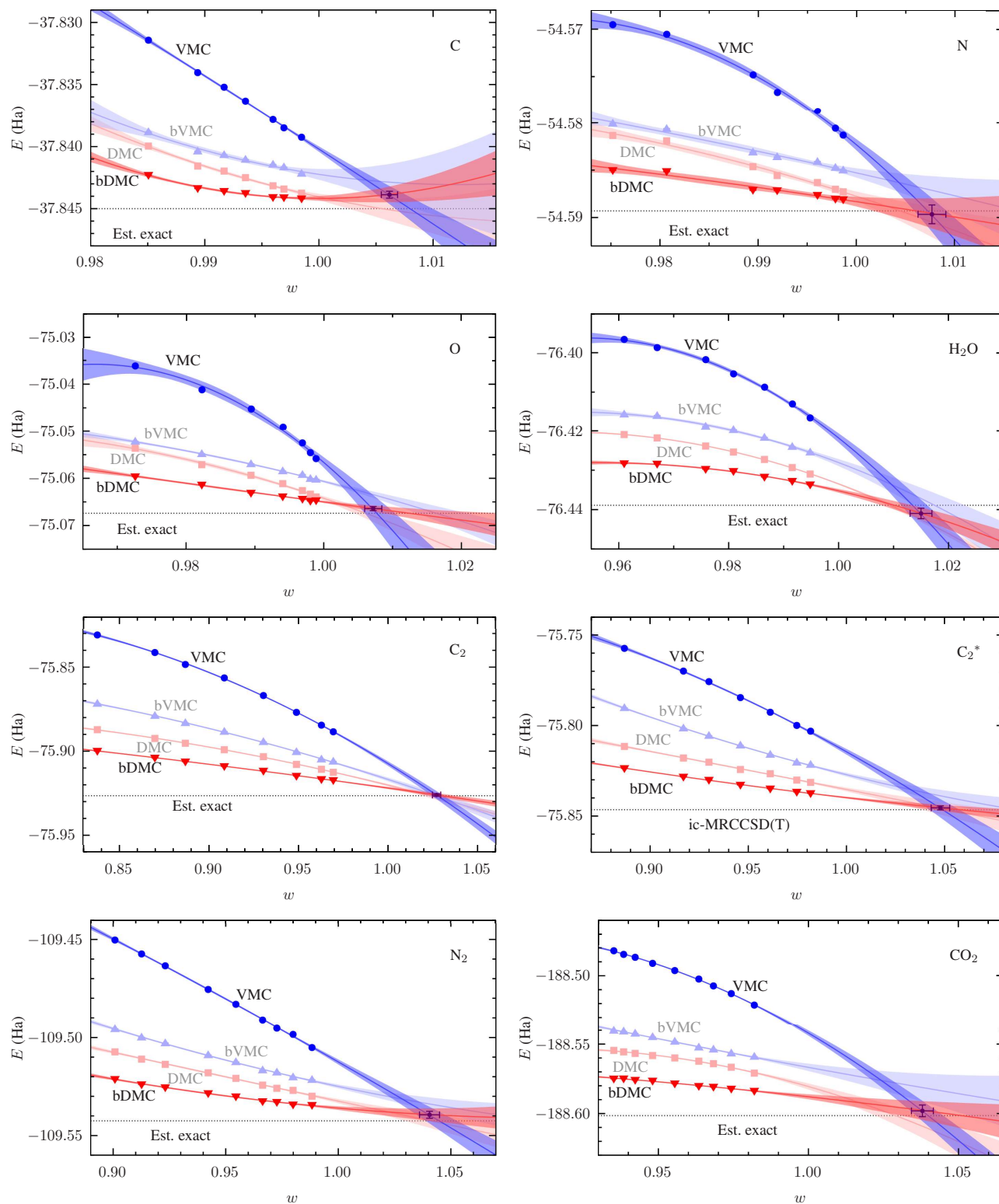


FIG. S1. VMC, DMC, bVMC, and bDMC energies of the atoms and molecules considered in this work as a function of w . Mean values of the fits to the data are shown as lines, and the translucent areas around them represent 95.5% (two-sigma) confidence intervals. Also shown in each plot is the relevant benchmark energy (see details in text and Table 4 of the manuscript) as a dotted line with a shaded area of ± 1 kcal/mol around it, and the intersection point between the VMC and bDMC curves.

S2. VALUES OF α

Table S9 shows the magnitude of the quasirandom fluctuations α estimated for each of the curves we have obtained, as defined in Eq. 7 of the manuscript. Note that all the individual cQMC calculations reported in Tables S1–S8 have been run for long enough that the statistical uncertainties on them are smaller than the corresponding value of α .

System	VMC	DMC	bVMC	bDMC
C	0.087	0.096	0.181	0.069
N	0.330	0.288	0.275	0.283
O	0.708	0.265	0.132	0.136
H ₂ O	0.408	0.020	0.302	0.144
C ₂	0.410	0.193	0.321	0.170
C ₂ *	0.508	0.339	0.325	0.136
N ₂	0.492	0.377	0.367	0.344
CO ₂	0.337	0.360	0.470	0.271

TABLE S9. Magnitude of the quasirandom error α for the VMC, DMC, bVMC, and bDMC curves used in our manuscript, in mHa.

S3. CONNECTION WITH SELECTED CI AND DMC VARIANCE EXTRAPOLATION

In selected CI methods one usually obtains the full-CI limit by extrapolates the total energy to the limit where the difference between the total energy and the variational energy (which typically amounts to a perturbation-theory correction) is zero.^{S1,S2} In the same spirit, one could consider extrapolating the DMC energy to the limit where the VMC-DMC energy difference is zero, which, by analogy with the selected CI approach, would effectively treat DMC as a perturbative correction of sorts on top of VMC.

Note that $E_{\text{VMC}} - E_{\text{DMC}}$ is proportional to the DMC variance,^{S3} so extrapolating to $E_{\text{VMC}} - E_{\text{DMC}} \rightarrow 0$ amounts to DMC variance extrapolation, analogous to VMC variance extrapolation schemes which have been used over the years, recent examples of which include Refs. S4 and S5.

One potential advantage of the DMC variance extrapolation approach over XSPOT is that the “exact” limit corresponds to a predefined value (zero) of the independent variable $E_{\text{VMC}} - E_{\text{DMC}}$, instead of an unknown value w_0 , so one does not need to explicitly intersect curves.

Clearly $E_{\text{VMC}} - E_{\text{DMC}} = 0$ implies that the VMC and DMC energy curves intersect as a function of w . From XSPOT, one can in fact derive that the DMC energy can be approximated by a second-order polynomial in $E_{\text{VMC}} - E_{\text{DMC}}$, but since w is eliminated in this process, the fit form for DMC variance extrapolation expresses no explicit assumptions on the dependence of the cQMC energies on the wave function. On the one hand, this is conceptually simpler, and could in principle avoid the orbital-basis exhaustion issue of the XSPOT method, since if both the VMC and DMC curves exhibit plateaus as functions of w then the DMC variance extrapolation curve may stall but need not deform. On the other hand, the explicit assumptions made by XSPOT could result in useful restrictions that guide the fits and reduce the uncertainty on the final results, an improvement that DMC variance extrapolation would miss on.

We have applied DMC variance extrapolation to our non-backflow and backflow data using the same fitting methodology we have used for XSPOT and in Fig. S2 we show the resulting fits. The energy data exhibit significant curvature, justifying the need for the quadratic fitting function, and our quasirandom fluctuation analysis produces values of α of the same order of magnitude as with XSPOT. We find that, for the most part, DMC variance extrapolation works, but yields much larger uncertainties than XSPOT. This is likely the case due to the data points being less evenly-spaced and often clustering together, resulting in several fits with non-monotonic mean values. It is noteworthy that the non-backflow and backflow curves do not line up in any of the cases, which one might expect them to since the extrapolation method is in principle agnostic to the specifics of the wave function.

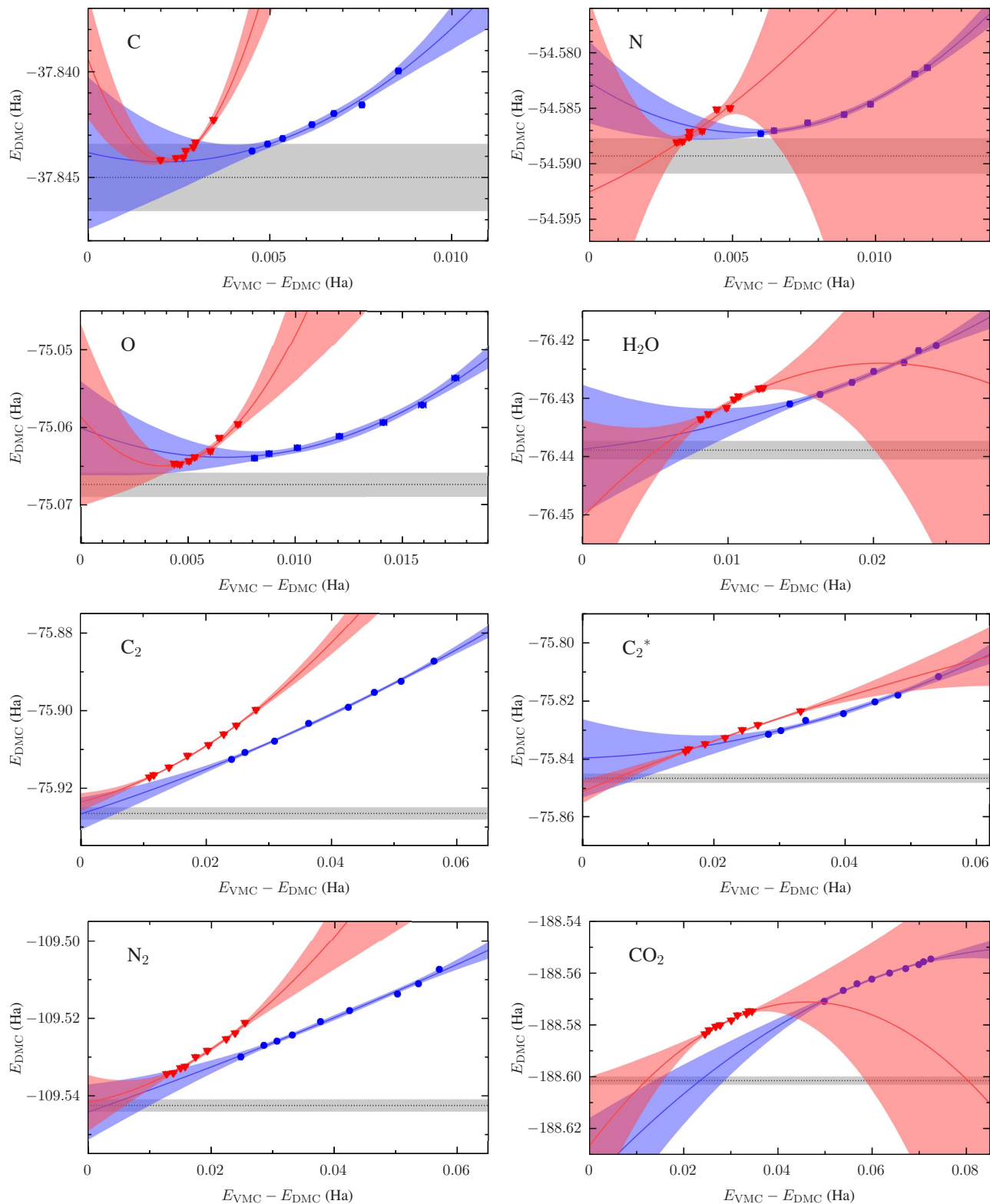


FIG. S2. Non-backflow (blue circles) and backflow (red triangles) DMC energy as a function of the corresponding VMC-DMC energy difference for the atoms and molecules considered in this work. Mean values of the fits to the data are shown as lines, and the translucent areas around them represent 95.5% (two-sigma) confidence intervals. Also shown in each plot is the relevant benchmark energy as a dotted line with a shaded area of ± 1 kcal/mol around it.

We have also applied DMC variance extrapolation to H₂O with natural orbitals, see Fig. S3, to see if the w -independent character of this approach gets around the orbital-basis exhaustion problem encountered by XSPOT, as mentioned above. We

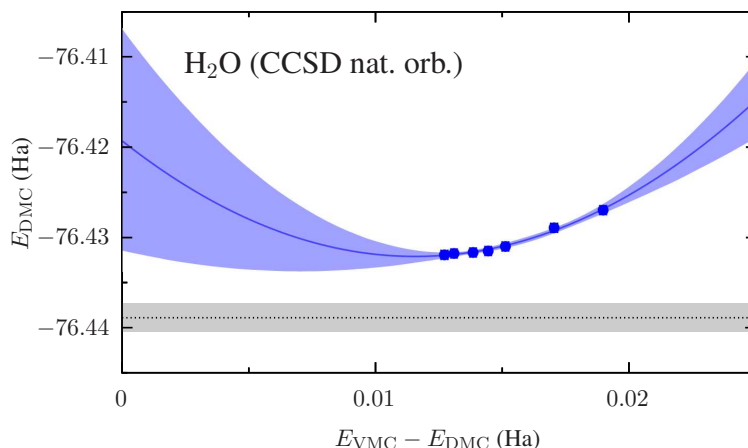


FIG. S3. DMC energy as a function of the VMC-DMC energy difference for H₂O using CCSD natural orbitals. The mean value of the fit to the data is shown as a line, and the translucent area around it represents the 95.5% (two-sigma) confidence interval. Also shown is the benchmark energy as a dotted line with a shaded area of ± 1 kcal/mol around it.

find that, in contrast with XSPOT which fails to produce an intersection as shown in Fig. 6 of the manuscript, DMC variance extrapolation does yield an energy estimate, but it is affected by a significant uncertainty and misses the benchmark by just over three sigma, which is overall a worse-quality result than when Hartree-Fock orbitals are used.

While DMC variance extrapolation has its merits, we believe that the XSPOT method we present in our manuscript is a superior option when applicable.

[S1]A. A. Holmes, C. J. Umrigar, S. Sharma, *Excited states using semistochastic heat-bath configuration interaction*, *J. Chem. Phys.* **147**, 164111 (2017).

[S2]H. G. A. Burton, P.-F. Loos, *Rationale for the extrapolation procedure in selected configuration interaction*, *J. Chem. Phys.* **160**, 104102 (2024).

[S3]D. M. Ceperley, *The statistical error of Green's function Monte Carlo*, *J. Stat. Phys.* **43**, 815 (1986).

[S4]M. Taddei, M. Ruggeri, S. Moroni, and M. Holzmann, *Iterative backflow renormalization procedure for many-body ground-state wave functions of strongly interacting normal Fermi liquids*, *Phys. Rev. B* **91**, 115106 (2015).

[S5]W. Fu, W. Ren, and J. Chen, *Variance extrapolation method for neural-network variational Monte Carlo*, *Mach. Learn.: Sci. Technol.* **5**, 015016 (2024).